ELSEVIER

Journal of Alloys and Compounds 404–406 (2005) 327–331

Journal of ALLOYS AND COMPOUNDS

www.elsevier.com/locate/jallcom

Microstructural effects in the hydrogenation kinetics of commercial-type $LaNi_5$ alloy

J.R. Ares*, F. Cuevas, A. Percheron-Guégan

Laboratoire de Chimie Métallurgique des Terres Rares, ISCSA-CNRS, 2-8 rue Henri Dunant, 94320 Thiais Cedex, France

Received 30 August 2004; accepted 19 January 2005
Available online 7 July 2005

Abstract

The influence of amorphous and nanocrystalline microstructures on the H-thermodynamics and kinetics of commercial-type $AB_{5.2}$ alloys have been investigated. On thermodynamic properties, amorphous phase exhibits a H-capacity reduction as compared to that of polycrystalline alloy. As concerns to kinetic properties, amorphous phase leads to slow kinetics which is controlled by hydrogen diffusion. Nanocrystalline alloy exhibits a slight capacity reduction as compared to polycrystalline which is related to a slopped plateau pressure. H-kinetics of nanocrystalline alloy is faster than both amorphous and polycrystalline alloys. The rate limiting step for the absorption kinetics in nanocrystalline alloy changes during hydrogen uptake from hydrogen diffusion to α/β phase transformation.

Keywords: Hydrogen storage materials; Intermetallics; Amorphous materials; Nanostructures; Gas–solid reactions

1. Introduction

During last decades, scientific research on batteries for portable devices has increased considerably [1]. Among other commercialised batteries (Ni–Cd, ion–lithium), the nickel–metal hydride (Ni–MH) battery is widely present in the market since the 90's [2]. It is based on the hydrogen transport between a negative electrode (metal hydride-based) and a positive electrode (NiOOH-based). The negative electrode is constituted of a polycrystalline alloy with AB_5 (A = rare earth, B = early transition metal) composition that absorbs and desorbs hydrogen easily. However, Ni–MH batteries exhibit slow hydrogenation kinetics for being used in high power applications.

Hydrogen kinetics in metal and alloys occurs through two main stages [3]: (i) a first step related to surface reactions (physisorption and chemisorption) and a second step concerning bulk phenomena: H-diffusion and phase transformation. Therefore, kinetics can be improved by different methods: (i) enhancement of surface reactivity by adding catalysts (Pt, Pd) [4], (ii) diminution of particle size to reduce long-range diffusion paths, and (iii) production of metastables phases, such as nanocrystalline and/or amorphous phases, with high H-diffusion coefficients [5].

At present, the influence of non-equilibrium microstructures on H-kinetics has been investigated in several intermetallic compounds. For example, recent investigations about Fe–Ti and Mg–Ni [6] alloys have shown an enhancement of H-kinetics when alloys have nanocrystalline and/or amorphous phases. As far as we know, the reasons of this effect have not so far been clarified. It is known that H diffusion at high hydrogen concentrations is faster for amorphous than polycrystalline materials [7]. In the case of nanocrystalline compounds, the great density of grain boundaries may have a major effect on long-range diffusion. Nevertheless, H-diffusion through grain boundaries will depend of the specific inter-grain structure. Also, nanocrystallite-size effects and the presence of defects [8] must influence the H-thermodynamic and H-kinetic properties of the alloy.

For AB_5 alloys, recent investigations [9] have shown that nanocrystalline and amorphous microstructures lead to lower H-capacities as compared to polycrystalline ones. As concerns to kinetics, the influence of these microstructures on hydrogenation rates and rate limiting steps (RLS) has not

* Corresponding author. Tel.: +33 49 415287 2565; fax: +33 49 415287 2625.
E-mail address: Jose.Ramon.Ares.Fernandez@gkss.de (J.R. Ares).

0925-8388/$ – see front matter © 2005 Elsevier B.V. All rights reserved.
doi:10.1016/j.jallcom.2005.01.110

been much investigated. In AB_5 polycrystalline alloy, the RLS depends drastically on the experimental conditions (H-pressure, temperature, number of activation cycles and alloy composition). In spite of this, it is commonly accepted that the RLS is H-diffusion at low pressures, whereas it turns to be hydride nucleation and growth at high pressures [10,11].

In this work, we study the role played by nanocrystalline and amorphous phases in commercial AB_5-type alloys as concerns, mainly, to hydrogenation kinetics.

2. Experimental

An alloy with nominal composition $La_{0.57}Pr_{0.27}Nd_{0.18}Ce_{0.04}Ni_{3.95}Mn_{0.4}Al_{0.3}Co_{0.55}$ ($AB_{5.2}$-stoichiometry) was prepared by induction-melting of pure metals (99.9%). This alloy is denoted as IM. It was then mechanically milled (initial particle size $<75\,\mu m$) in a Fritsch P7 planetary device. Milling was done under argon atmosphere at a vial rotation speed of 740 rpm for 48 h. Stainless steel balls of 7 mm in diameter were used with a ball to powder mass ratio 10:1. The obtained sample was denoted as MM. The milled powders were cold pressed at 80 MPa and subsequently annealed under argon atmosphere at 325 °C (A1 sample) and 475 °C (A2 sample) during 1 h.

Structural properties of the four samples were investigated at room temperature by X-ray diffraction using a Bruker AXD D8 θ–θ diffractometer equipped with Cu Kα radiation. Diffraction patterns were analysed by the Rietveld method using the FullProf software [12]. Pressure-composition isotherms (PCI) were obtained at 55 °C in a Sievert's-type device. H-absorption and desorption kinetic curves were performed at 55 °C in the same device under a quasi-constant hydrogen pressure of 0.9 MPa and 0.01 MPa, respectively.

Thermal analyses were done in a differential scanning calorimeter (DSC-Q100) from TA instruments. Heating runs were carried out under He flow at 20 °C/min from 40 to 500 °C.

3. Results and discussion

3.1. Microstructural analysis

Fig. 1 shows the XRD patterns of the induction-melted sample (IM), the sample milled for 48 h (MM) and the samples subsequently annealed at 325 °C (A1) and 475 °C (A2). All patterns can be well fitted with a $CaCu_5$-type structure. In addition, MM and A1 samples exhibit a broad diffraction bump between 30° and 50° denoting the existence of an amorphous phase. The amount of this phase can be roughly estimated from the ratio of the integrated intensity of the diffraction bump to that of the whole diffraction pattern (Table 1). On the contrary, IM and A2 samples exhibit a flat diffraction background. Good Rietveld fittings are obtained for all samples (Rwp < 12%). Microstructural properties for the four samples as obtained by Rietveld analysis are summarised in Table 1. IM is single-phase and polycrystalline with a crystallite size of ∼2000 Å. MM and A1 are biphasic (nanocrystalline + amorphous). The amount of amorphous phase in A1 as compared to MM is reduced by the annealing treatment. After the high temperature annealing treatment (A2 sample) amorphous phase is eliminated and the crystallite size increases slightly (from 80 to 90 Å). As concerns to the lattice

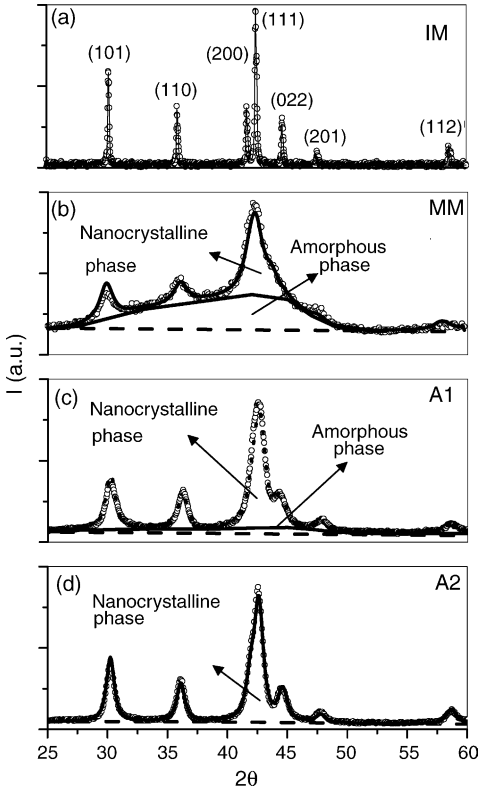

Fig. 1. XRD patterns of (a) IM sample, (b) milled sample (MM), (c) sample annealed at 325 °C (A1), (d) sample annealed at 475 °C (A2). All diffraction peaks were fitted with a $CaCu_5$-type structure.

Table 1
Microstructural parameters for all studied samples

Sample	Microstructure	D_V (Å)	ε (%)	a (Å)	c (Å)	V (Å^3)
IM	Polycrystalline	2000(50)	0.05 (1)	4.999 (1)	4.0569 (1)	87.80 (1)
MM	Amorphous (60%) + nanocrystalline (40%)	50(20)	0.5 (2)	4.983 (4)	4.1467 (5)	89.2 (2)
A1	Amorphous (15%) + nanocrystalline (85%)	80(10)	0.60 (3)	4.956 (9)	4.0818 (9)	86.83 (4)
A2	Nanocrystalline	90(10)	0.42 (3)	4.9746 (7)	4.062 (7)	87.05 (1)

D_V: crystallite size; ε: lattice strain; a and c and V: lattice parameters and unit cell volume, respectively—obtained by Rietveld analysis.

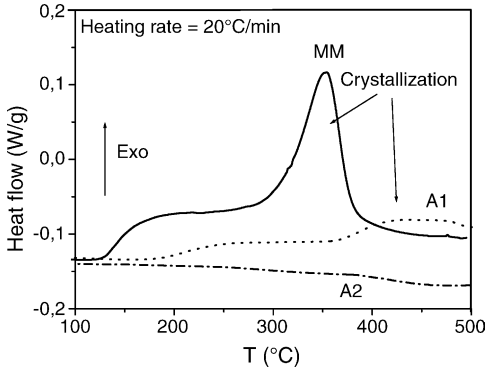

Fig. 2. DSC measurements of milled sample (MM), sample annealed at 325 °C (A1) and sample annealed at 475 °C (A2).

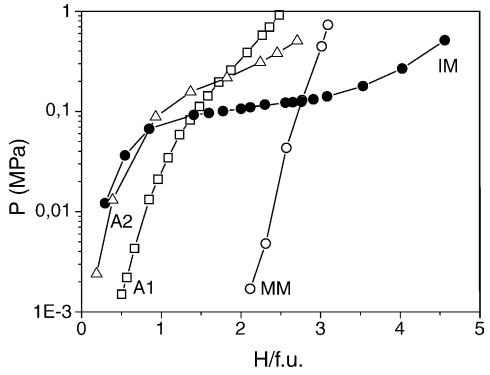

Fig. 3. PCI absorption curves at 55 °C of induction-melted sample (IM), milled sample (MM), sample annealed at 325 °C (A1) and sampled annealed at 475 °C (A2).

parameters, a significant diminution of the *c* parameter occurs while milling and is recovered after the annealing treatment. This effect has been attributed to atomic-site interchange between A-type and B-type atoms as reported elsewhere [13].

To obtain more information about the content and stability of the amorphous phase, DSC measurements have been carried out and are shown in Fig. 2. MM exhibits an exothermic peak at 354 ± 1 °C with an energy of 30 ± 1 J/g related to the crystallization of the amorphous phase. Besides, a wide band from 150 to 400 °C is detected. This band could be attributed to amorphous relaxation [14] as well as to the enthalpy stored in crystallite boundaries [15].

Sample annealed at lower temperature (A1) also exhibits a crystallization peak but with less intensity as compared to MM in agreement with its lower amorphous content (Table 1). The crystallization peak is at $T = 450 \pm 10$ °C what seems to indicate different short-range order for the amorphous phase in A1 as compared to MM. Also, a wide band (from 200 to 450 °C) is here detected. On the contrary, A2 sample does not show any peak which indicates a complete amorphous crystallization after annealing at 475 °C.

Finally, Scanning Electron Microscopy observations show that the annealing treatment does not modify the sample particle size obtained after milling. Milled and annealed samples exhibit a particle size of 25 ± 5 μm [9].

3.2. PCI isotherms

Fig. 3 shows the PCI absorption curves at 55 °C for the four samples. IM sample exhibits a wide plateau pressure at 0.1 MPa which extends from 0.8 to 3.2 hydrogen atoms per alloy formula unit (H/f.u.). On the contrary, MM sample does not exhibit any plateau pressure and has a high solubility at low pressure. On annealing, H-solubility at low pressure is reduced (A1 and A2) and a slopping plateau appears after annealing at 475 °C (A2). It has been reported that amorphous materials possess a continuous distribution of trapping sites for hydrogen atoms [16]. Thus, the observed decrease in solubility at low H-concentration for A1 and A2 samples could be explained by the reduction of the amount of amorphous phase on annealing [13]. These trapped sites have been previously characterised by thermal desorption [9]. The fact that nanocrystalline alloys do not display a flat plateau pressure may be related to different potential energies for hydrogen atoms inside the nanocrystallites and in the vicinity of grain boundaries. This would cause a certain energy distribution hydrogen sites around that corresponding to the plateau energy [17]. As a consequence, H-capacity at high pressures (>0.1 MPa) is reduced in nanocrystalline as compared to polycrystalline alloy. It should be noted that the plateau pressure of A2 alloy is higher than that of IM alloy. This may be related to the bigger cell volume exhibited by IM alloy (87.80 Å^3) as compared to A2 alloy (87.05 Å^3). It is well known that in AB_5-type alloys there is a linear relation between the intermetallic cell volume and the logarithm of the plateau pressure [18].

3.3. Kinetic analysis

Hydrogenation curves for MM, A1 and A2 samples are shown in Fig. 4. In all cases, absorption reactions are observed to be faster than desorption ones. In Table 2 absorption/desorption time to reach a reacted fraction of 0.8 ($t_{F=0.8}$) is given. The fastest kinetics is obtained for the sample annealed at the highest temperature (A2). For example, during absorption $t_{F=0.8}$ is reached in 80 s for A2 sample, whereas it takes 2600 s for MM. sample. As concerns IM sample (not shown in Fig. 4 for a better comparison between the other samples) much slower kinetics have been determined ($t_{F=0.8} = 4000$ s for absorption and $t_{F=0.8} = 15000$ s). This result agrees with previous reports on the improvement of hydrogenation kinetics after milling treatments [6]. However, a significant reduction of the alloy particle-size on milling rather than the induced modifications in the alloy microstructure may be at the basis of this effect. In our case, the particle size for the IM sample was ∼70 μm, i.e. three times higher than that obtained after mechanical milling (25 μm). A meaningful kinetic comparison between IM and milled samples as concerns the influence of the alloy microstructure is, therefore, difficult to provide. Thus, no further comparison will be

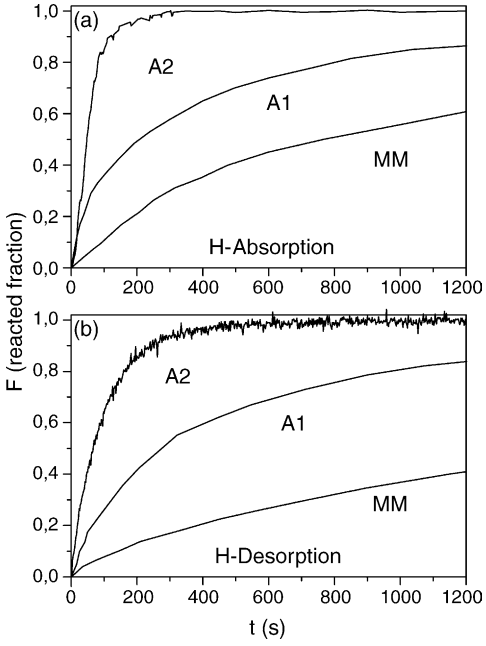

Fig. 4. Time evolution of the reacted fraction (F) in MM, A1 and A2 samples during, (a) H-absorption and (b) H-desorption. Hydrogenation pressures during absorption and desorption experiments were 0.9 and 0.01 MPa, respectively.

here made between IM and milled samples. Nevertheless, an exhaustive kinetic study of the RLS for AB_5-type polycrystalline alloys is presented in an accompanying publication [19].

To determinate which mechanism controls the H-kinetics in milled samples, a method described in [20] was used. This method compares the hydrogenation curves with solid-state rate equations related to different rate limiting steps (RLS): diffusion and phase transformation mechanisms. The method produces linear plots ($(\ln - \ln(1 - F))$ versus $\ln t$) with constant slope m. As summarized in Table 3, the resulting m-value gives information on the controlling reaction mechanism according to different theoretical equations.

Fig. 5 shows the result of this analysis as concerns to MM, A1 and A2 samples for both hydrogen absorption and desorption kinetics. The obtained m-values are summarized in Table 2. In samples with amorphous phase (MM and A1), m-values for both absorption and desorption reactions are within the range 0.7–0.8. Then, according to Table 3, the RLS seems to be a mixed control between phase transformation (either α/β nucleation at the surface (F1) or α/β inter-phase displacement (R3)) and diffusion (D3). This fact may be related to the existence of two phases in the alloys (amorphous and nanocrystalline phases) whose kinetics are controlled by different mechanisms: H-diffusion for the amorphous phase

Table 2
Absorption/Desorption time to reach a reaction fraction of $F = 0.8$ in MM, A1 and A2 samples and determined m-values

Sample	$t_{F=0.8}$ (s) Absorption	$t_{F=0.8}$ (s) Desorption	m-values Absorption	m-values Desorption
MM	2600	6000	0.80 ± 0.02	0.71 ± 0.02
A1	800	1000	0.71 ± 0.02	0.72 ± 0.02
A2	80	400	$0.55 \pm 0.20/1.45 \pm 0.05$[a]	0.90 ± 0.02

[a] Two m-values are observed during H-absorption in A2.

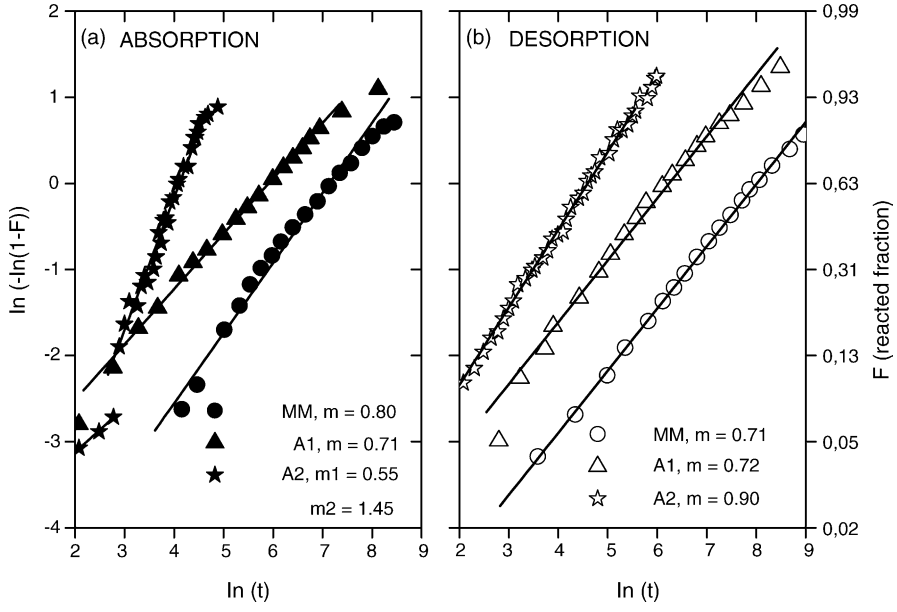

Fig. 5. Plots of $\ln(-\ln(1 - F))$ vs. $\ln t$ for MM, A1 and A2 samples for (a) H-absorption and (b) H-desorption. Linear fits to the data with slope m are shown by continuous lines.

Table 3
Rate equations related to different RLS and the corresponding m-values of the linear relationship $\ln(-\ln(1-F)) = \text{constant} + m\ln t$

Function	Equation	m-Values	RLS
D3(F)	$[1-(1-F)^{1/3}]^2 = kt$	0.54	H-Diffusion
F1(F)	$-\ln(1-F) = kt$	1	Nucleation at the surface
R3(F)	$1-(1-F)^{1/3} = kt$	1.07	Interphase displacement
A2(F)	$[-\ln(1-F)]^{1/2} = kt$	2	Bulk nucleation and Growth in 2D
A3(F)	$[-\ln(1-F)]^{1/3} = kt$	3	Bulk nucleation and growth in 3D

F = reacted fraction, t = time.

and α/β phase transformation for the nanocrystalline phase. Kinetic rates in A1 are faster than in MM (Fig. 4) which indicates slower kinetics for the amorphous phase as compared to the nanocrystalline one. This could be explained by a low hydrogen diffusion coefficient in amorphous $AB_{5.2}$ alloy at the studied H-concentrations.

For the sample without amorphous phase (A2), kinetics is more complex. During absorption, two m-values were obtained: $m = 0.55$ (at short time, $t < 20$ s) and $m = 1.45$ (at long time, $t > 20$ s). Accordingly, H-diffusion is assigned to be the RLS at small reacted fraction ($F < 0.1$), whereas an α/β phase transformation mechanism governs hydrogen absorption at higher reacted fraction ($F > 0.1$). First reaction stage may be tentatively ascribed to H-diffusion in nanocrystalline grain boundaries, whereas the second one is attributed to two-dimensional nucleation and growth of β-hydride inside of the nanocrystallites. During desorption, a mechanism of phase transformation seems to be predominant ($m = 0.90$), which may be related either to the nucleation of the α phase at the surface or to the displacement of the α/β inter-phase.

4. Conclusions

Microstructural effects on thermodynamic and kinetic properties of AB_5 type alloys have been investigated. The occurrence of amorphous phase leads to a strong capacity reduction accompanied by an absence of plateau pressure. Detrimental effects are also observed as refers to H-kinetics. They are sluggish, what seems to be related to a low H-diffusivity in the amorphous phase. Nanocrystalline phase also reduces the H-capacity of AB_5 alloys, though to a lower extent, and produce a slopped plateau pressure. However, H-kinetics is much improved in the nano-crystalline phase presumably due to fast H-diffusion through grain boundaries.

Acknowledgements

Authors wish to thank F. Briaucourt for technical assistance.

References

[1] C.K. Dyer, J. Power Sources 106 (2002) 31.
[2] F. Feng, M. Geng, D.O. Northwood, Int. J. Hydrogen Energy 26 (2001) 725.
[3] M. Martin, C. Gomel, C. Borkhart, E. Fromm, J. Alloys Compd. 238 (1996) 193.
[4] V.M. Gryaznov, Platinum Met. Rev. 36 (1992) 70.
[5] V.V. Kondratyev, A.V. Gapontsev, A.N. Voloshinskii, A.G. Obukhov, N.I. Timofeyev, Int. J. Hydrogen Energy 24 (9) (1999) 819.
[6] L. Zaluski, A. Zaluska, J.O. Strom-Olsen, J. Alloys Compd. 253 (1997) 70.
[7] R. Kirchheim, T. Mütsele, W. Kieninger, H. Gleiter, R. Birringe, T.D. Koble, Mater. Sci. Eng. 99 (1988) 457.
[8] T. Kuji, Y. Matsumura, H. Uchida, T. Aizawa, J. Alloys Compd. 330–332 (2002) 71.
[9] J.R. Ares, F. Cuevas, A. Percheron-Guégan, Mater. Sci. Eng. B 108 (2004) 76.
[10] X.H. Wang, C.S. Wang, Y.Q. Lei, C.P. Chen, Q.D. Chang, Int. J. Hydrogen Energy 21 (6) (1996) 471.
[11] C.S. Wang, X.H. Wang, Y.Q. Lei, C.P. Chen, Q.D. Chang, Int. J. Hydrogen Energy 21 (6) (1996) 479.
[12] J. Rodriguez-Carvajal, Physica B 192 (1993) 55.
[13] J.R. Ares, F. Cuevas, A. Percheron-Guégan, Acta Mater. 53 (2005) 5157.
[14] S. Ram, Phys. Rev. B 42 (1992) 9582.
[15] C. Suryanarayama, Prog. Mater. Sci. 46 (2001) 1.
[16] N. Mommer, M. Hirscher, F. Cuevas, H. Kronmuller, J. Alloys Compd. 266 (1998) 255.
[17] R. Kirchheim, F. Sommer, G. Schluckebier, Acta Metall. 30 (6) (1982) 1059.
[18] J.-C. Achard, A. Percheron-Guégan, H. Diaz, F. Briaucourt, F. Demany, Proceedings of the Second International Congress on Hydrogen in Metals, Paris, 1977, p. 1E12.
[19] E. Raekelboom, F. Cuevas, B. Knosp, A. Percheron-Guégan, J. Alloys Compd., submitted for publication.
[20] J.D. Hancock, J.H. Sharp, J. Am. Cer. Soc. 55 (1972) 75.